A Letters Journal Exploring the Frontiers of Physics

June 2017

EPL, **118** (2017) 56005 www.epljournal.org
doi: 10.1209/0295-5075/118/56005

Surface creasing of soft elastic continua as a Kosterlitz-Thouless transition

T. A. Engstrom[(a)] and J. M. Schwarz[(b)]

Soft Matter Program and Department of Physics, Syracuse University - Syracuse, NY 13244, USA

received 9 May 2017; accepted in final form 20 July 2017
published online 11 August 2017

PACS 68.35.Rh – Solid surfaces and solid-solid interfaces: structure and energetics: Phase transitions and critical phenomena
PACS 46.05.+b – General theory of continuum mechanics of solids
PACS 87.15.Zg – Biomolecules: structure and physical properties: Phase transitions

Abstract – Harnessing a model from composite materials science, we show how microscopic crease and anticrease features may arise as quasi-particle excitations on the surface of a soft elastic material, where disorder and drive-induced strain fluctuations play the role of thermal fluctuations. These features appear above a critical strain fluctuation at which zero-length crease-anticrease pairs unbind, analogous to vortex unbinding in the Kosterlitz-Thouless transition. Finite-length creases can be described in the same framework. Our predictions for crease surface profiles and onset strain agree with previous experiments, and further tests are proposed.

Cusped inward folds known as creases form on compressed surfaces of a variety of soft elastic materials [1], including natural rubber [2,3], polymer gels [4–6], silicone elastomers [7–13], starchy foods [14,15], and the developing mammalian brain [11,12,16,17]. In the latter context, creases are called "sulci". Unlike the long-wavelength buckling of a compressed beam, or the smooth sinusoidal wrinkles observed on the skin of drying fruit or a tensioned elastic sheet [18–20], creases are sharply localized in both their elastic deformation and stresses, thereby defying a linear perturbation analysis [3,7,14,21,22]. Owing to this difficulty, little progress has been made toward an analytical understanding of creases. Instead, numerical minimization of a nonlinear neo-Hookean energy functional has become the standard theoretical tool for investigating their onset [7,11–14,16,21–23]. A central claim in much of this work is that creasing is a fundamentally new, nonlinear instability with no scale [21,22]. Experimental work has also studied the growth of pre-existing long creases, describing these behaviors in analogy to crack propagation [8,9].

Typically, the microstructure of a creaseable material consists of a random network of crosslinked, flexible or semiflexible polymer chains. Elastic moduli of such materials are spatially inhomogeneous, giving rise to non-affine distortions (fluctuations), upon macroscopic deformation [24,25]. Under large strains such as those required to initiate creasing, the RMS amplitude of these fluctuations can be comparable to the dimensions of the newly formed creases. For example, embedded tracer particles reveal non-affine displacements in sheared polyacrylamide gel of order 0.3 micron at strains $\sim$35% [25], while fully developed creases can be at least as small as $\sim$1 micron wide $\times$3 micron long in the same material [5], and numerical energy minimization indicates that crease size goes to zero at the critical point [22]. Simulations invoke surface perturbations of one form or another to trigger crease formation [7,11,13,16,22], but otherwise treat crease formation as a statics problem; in planar geometry, the creased state is found to have lower elastic energy than the flat state for uniaxial compressive strain $> 35\%$ [14,22] or equibiaxial strain $> 27\%$ [16]. (Compare the experimentally measured critical strains for these two cases: 32–38% [13] and $33 \pm 2\%$ [5], respectively.) While this statics approach is appealing for *macroscopic* creases, and yields additional predictions for surface profiles and crease patterns that agree with experiments [7,16], the neglect of fluctuations appears to be unrealistic in the regime of *microscopic* creases, *i.e.*, those near creasing onset. In this regime, the notion of a flat reference state (relative to the size of the crease) is called into question.

[(a)] E-mail: taengstr@syr.edu
[(b)] E-mail: jmschw02@syr.edu

A crease characterized by strains $\epsilon \sim 1$ within a volume $V \sim (0.3 \text{ micron})^3$ would be a strongly athermal object; in polyacrylamide with shear modulus $G \sim 1\,\text{kPa}$, its elastic energy would be of order $GV\epsilon^2 \sim 10^4 k_B T$. Here, however, we consider the possibility that compression-induced, non-affine fluctuations can act as an "effective temperature," endowing a micro-crease with an "effective entropy". This viewpoint leads to a novel mechanism for the formation of micro-creases that can be regarded as precursors to macro-creases. Furthermore, the essential features of our proposed micro-creasing mechanism are amenable to simple analytic calculations, by virtue of a domain decomposition that relegates nonlinear elasticity to small, energetically inconsequential regions analogous to vortex cores.

The main content of this letter is a new quasi-particle framework for shear stress focusing in soft solids, assuming planar geometry and neglecting surface tension. We consider the formation of micro-creases from within this framework, finding evidence that i) creasing onset maps to the Kosterlitz-Thouless (KT) transition [26], ii) nonlinear deformations can be decoupled from linear, and iii) compression-induced shear strain fluctuations set the fundamental, microscopic lengthscale in the problem. Our theory makes contact with experimental results on critical strain and crease surface profiles. In particular, we obtain a universal critical compressive strain $\epsilon_c \approx 30\%$ above which creases emerge. Finally, the theory points to a set of minimal physical ingredients for creasing, and suggests a possible unification with ridging (formation of localized surface protrusions) [27], and dimple crystallization [28,29].

Our point of departure from prior work is to consider a distinct regime of zero-length creases, qualitatively similar to those observed in [6–8], immediately upon nucleation, and those in [16], as the critical point is approached from above. Deformations reminiscent of these zero-length creases also appear in a very different continuum elastic context, namely the shear lag model of composite materials science and engineering [30,31]. In this model, which will become foundational to our theory of micro-creasing, one assumes that shear coupling is supported at the interface between a low-dimensional reinforcing phase (*i.e.*, 1d fibers or 2d slabs) and a surrounding 3d matrix phase. Next, an approximation is made that the transfer of axial loads between the two components is accomplished entirely via tension or compression in the reinforcing phase, and pure shear in the matrix. Axial loads refer to external or internal forces (such as those arising from differential growth of the two components) acting parallel to a long axis of the reinforcing phase. In the case of a fiber-matrix composite, the model predicts that matrix shear stress and strain fall off as $1/r$, where r is the perpendicular distance from a fiber. Thus, the matrix deformation and hence the surface profile scales as $\ln r$ (see fig. 1).

Mapping shear lag to 2d electrodynamics. – Let us take all forces in the shear lag model along z. In the matrix phase, the only non-negligible components of the strain tensor $\epsilon_{ij} = (\partial_i u_j + \partial_j u_i)/2$ have one index equal to z and the other not equal to z. Defining a 2d vector of shear strains $\vec{\gamma} = 2(\epsilon_{xz}, \epsilon_{yz})$, force balance on a volume element of matrix takes the form of Gauss's law

$$\oint \vec{\gamma} \cdot \mathrm{d}\mathbf{A} = \frac{f_0}{G}. \tag{1}$$

Here G is the matrix shear modulus while f_0 is the net force supported at the interface and enclosed by the free-body diagram (Gaussian surface). In terms of the wetted perimeter $p_0(z)$ and interfacial shear stress $\tau_0(z)$, the interfacial force is $f_0 = \int \mathrm{d}z\, p_0 \tau_0$. Our neglect of ϵ_{zz} is justified by requiring $p_0\tau_0$ to vary slowly with z.

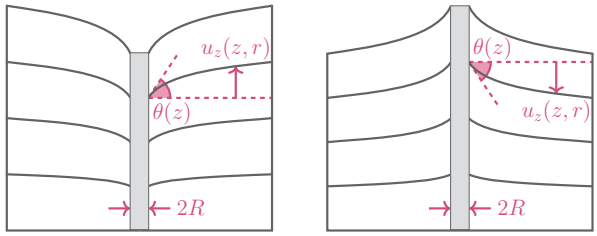

Fig. 1: (Colour online) Cartoon of axisymmetric shear lag. Curved lines indicate the matrix deformation $u_z \sim \tan(\theta)\ln(r/R)$ around an isolated vertical fiber of radius R (shaded). The left case shows a crease-like deformation that results when the fiber is under axial tension; the right case shows an anticrease-like deformation resulting from a fiber under compression. As depicted, both the equilibrium length of the fiber and the pre-deformed matrix height are shorter in the left case than in the right case.

Equivalently, one has a Poisson's equation for the (scalar) deformation field u_z. For the important special case of a thin fiber source at the origin,

$$\nabla_r^2 u_z(z, \mathbf{r}) = 2\pi R \tan(\theta(z))\delta^2(\mathbf{r}), \tag{2}$$

where R is the fiber radius and $\tan\theta = \tau_0/G$ is the interfacial shear strain, as indicated in fig. 1. $2\pi R \tan\theta$ is the "charge" per unit length of fiber. (Note that in the case of a viscoelastic matrix with storage and loss moduli given by G' and G'', respectively, a frequency-dependent "dielectric function" appears as $1 + iG''/G'$.) The solution of eq. (2) is

$$u_z(z, \mathbf{r}) = -2\pi R \tan(\theta(z)) C(\mathbf{r}), \tag{3}$$

where $C(\mathbf{r}) = -\ln(|\mathbf{r}|/R)/2\pi$ is the 2d Coulomb potential (Green's function).

Guided by this mapping, we ask whether u_z might be associated with a quasi-charge excitation in which the fiber of the conventional shear lag model is an abstraction. For system size L and vertical thickness h, the elastic strain energy (electrostatic energy) $\frac{G}{2}\int \mathrm{d}V\, \gamma^2$ required to create an isolated such "ghost fiber" is

$$U_{\text{gf}} = E_{\text{core}} + \pi G h R^2 \overline{\tan^2\theta} \ln(L/R). \tag{4}$$

The overbar denotes an average over z, and the core contribution is from (possibly nonlinear) deformations within $r < R$. Notably, this result resembles the energy of an isolated vortex [32], and $\frac{G}{2}\gamma^2$ is a leading-order term of the energy density used in the aforementioned neo-Hookean simulations imposing an incompressibility constraint. Motivated thus, we now turn to the statistics of ghost fibers. (In what follows, the term "ghost fiber" will sometimes be used synonymously with crease (or anticrease, as the case may be), although it will be good to keep in mind that it most accurately refers to just the crease *core*, which is the fundamental charge-like entity.)

Effective thermodynamics of shear lag quasi-particles. – The central postulate of this work is that non-affine strain fluctuations generated during macroscopic deformation of a microscopically inhomogeneous material can play the role of thermal fluctuations. That is, there is an "effective temperature" that increases during a slow compression of an elastomer or gel, exciting ghost fiber quasi-particles out of the vacuum and enabling them to explore many configurations. Similar effective temperature approaches have been successfully used to describe the statistics of granular materials, pinned vortex lattices, artificial spin ice, and other athermal systems [33–37]. For example, agitating 2d artificial spin ice systems by rotating them in an external, decreasing magnetic field can yield "equilibrium" populations of different vertex types, despite the energy scale of spin flips being $\sim 10^5 k_B T$ [36].

With justification to follow, we give our effective temperature postulate as

$$k_B T_{\rm eff} \sim G\langle\epsilon_d^2\rangle \lambda_d^2\, l_d, \tag{5}$$

where $\langle\epsilon_d^2\rangle$ is the mean squared amplitude of ϵ_{xz} and ϵ_{yz} fluctuations, and λ_d, l_d are the characteristic wavelength and skin depth of these fluctuations. Equation (5) is reminiscent of the Lindemann criterion for bulk melting of a harmonic solid [38]. We will identify the effective system thickness h with l_d, below which the system is cold and inactive.

Working within the microcanonical ensemble, the configurational entropy of a system containing a single ghost fiber is $S = 2k_B \ln(L/R)$. The free energy cost to create the ghost fiber is $F = U_{\rm gf} - T_{\rm eff} S$. In the thermodynamic limit where the finite core energy is dominated by the logarithmically divergent term, $F < 0$ for mean square strain fluctuations greater than the critical value

$$\langle\epsilon_d^2\rangle_c = \frac{\pi}{2}\frac{R^2}{\lambda_d^2}\,\overline{\tan^2\theta}. \tag{6}$$

Because the quantity that maps to electric charge is an odd function of θ, a charge dipole corresponds to a crease-anticrease pair of surface deformations, alternatively viewed as a tension-compression pair of ghost fibers (see fig. 1). The energy required to create a pure dipole is finite, in contrast to eq. (4), and thus ghost fibers in 3d are analogous to vortices in 2d: for $\langle\epsilon_d^2\rangle < \langle\epsilon_d^2\rangle_c$, the system contains tension-compression bound pairs of ghost fibers, and at $\langle\epsilon_d^2\rangle_c$ there is an unbinding transition (KT transition).

We now consider the grand canonical ensemble. A charge neutral system of ghost fibers has Hamiltonian

$$H = \sum_i E_{{\rm core},i} + 4\pi^2 G h \sum_{i<j} R_i R_j \overline{\tan\theta_i}\,\overline{\tan\theta_j} C(\mathbf{r}_i - \mathbf{r}_j). \tag{7}$$

So long as any strong nonlinearities in the core are confined to $r \ll R$, simple scaling arguments indicate $E_{\rm core} \sim G V_{\rm core} \epsilon_{\rm core}^2 \sim Gh\pi R^2 (\overline{\tan\theta})^2$. This quantity would appear to vary from one quasi-particle to another because the charges $\sim R_i \overline{\tan\theta_i}$ are here continuous degrees of freedom. However, we can exploit the arbitrariness of the R_i in order to take the core energy as a meaningful chemical potential μ. The appropriate choice is $R_i = s|\overline{\tan\theta_i}|^{-1}$, where $s \sim \sqrt{\mu/(Gh\pi)}$. This brings the partition function into the Coulomb gas form

$$Z = \sum_{\{n_i\}} \int \prod_i {\rm d}^2 r_i \; y_0^{\sum_i n_i^2} e^{4\pi \ln y_0 \sum_{i<j} n_i n_j C(\mathbf{r}_i - \mathbf{r}_j)}, \tag{8}$$

where $n_i = \pm 1$ and $y_0 = \exp[-\mu/k_B T_{\rm eff}]$ is the ghost fiber fugacity. The price paid for replacing continuous charges with discrete ones is that R is now an ambiguous "lattice constant". However, we have made available a small and well-defined lengthscale s; this can presumably replace R as the short-distance cutoff.

The fugacity y_0 and "coupling constant" $K = -(\ln y_0)/\pi$ are related because we are considering a specific physical system (*e.g.*, ref. [32]). Intersection of the line $y_0 = e^{-\pi K}$ and the line of fixed points $y_0 = -\pi^{-2}(K^{-1} - \pi/2)$ determines the critical inverse coupling $K_c^{-1} = 1.06$, and hence the critical mean square strain fluctuation $\langle\epsilon_d^2\rangle_c = (s^2/\lambda_d^2) K_c^{-1}$. Note K_c^{-1} is depressed from the mean field value $\pi/2$ obtained earlier.

Below $\langle\epsilon_d^2\rangle_c$, large-scale surface deformation would not be seen because the tension-compression pairs are tightly bound. The appearance of spatially separated, cusped surface deformations at a critical point that has no explicit dependence on system thickness or shear modulus is consistent with creasing experiments [5]. So too, we argue from data in [6–8,16], is the notion of zero-length creases at the critical point. (But see [9] for a different interpretation of crease lengths.) In light of the apparently universal $\approx 33\%$ onset strain [5], and the omnipresent microscopic disorder, one is tempted to identify λ_d with the lattice constant s (possibly scaled by a numerical prefactor). In fact, the simulations of Tallinen *et al.* use random vertical displacements of mesh surface nodes [16], consistent with this picture. A crude estimate of the critical compressive plane strain ϵ_c can now be made, by approximating the shear strain fluctuations with a square wave with amplitude $\sqrt{\langle\epsilon_d^2\rangle}$, such that the corresponding fluctuations in vertical displacement are a triangular wave with amplitude

$\frac{1}{2}\lambda_d\sqrt{\langle\epsilon_d^2\rangle}$. This triangular waveform represents an idealized surface roughness profile arising from the non-affine displacements. We further assume conservation of the area of the free surface, *i.e.*, as the slab is compressed, the surface concertinas between stress concentrators. (Qualitatively similar roughening behavior has been observed for polycrystalline metal under compressive plane strain [39].) Setting the lattice constant s equal to the largest length-scale over which shear strain is constant in this model, namely $\lambda_d/2$, , we then find $\epsilon_c = 1-(1+K_c^{-1})^{-1/2} = 38\%$ (mean-field theory) and $= 30\%$ (renormalization group), which bracket 33%.

Ghost fibers in the post-transitional regime. – Two important features of creasing experiments remain to be explained by our quasi-particle theory: i) that only creases and not anticreases appear to be seen, and ii) that zero-length creases smoothly become finite-length creases. In this section we consider i), and in the next section we will consider ii).

The KT transition does not involve (or at least, does not require) self-contact in the core region. Yet self-contact is generically observed [7,8,14,16,22]. We propose that self-contact ensues at strain $\epsilon_{sc} > \epsilon_c$, and point out that it can only be available to creases, because a self-contacting anticrease is an unphysical concept. Anticreases should therefore incur a higher-energy penalty than creases, in the regime $\epsilon > \epsilon_{sc}$, because they are not as effective at sequestering surface area (thus material near the surface must be compressed to a greater extent). The system cannot exactly get rid of its anticreases, though. Doing so would generate a non-zero net charge, causing u_z to grow with system size as $(\sum_i n_i)\ln L$, clearly inconsistent with experiments. What happens, we propose, is that an anticrease's R increases while its $|\overline{\tan\theta}|$ decreases, in such a way that its charge $-2\pi R|\overline{\tan\theta}|$ stays fixed. In other words, the negative point charges get smeared out into a negative background charge (cf. the non-neutral Coulomb gas [40]). The Poisson equation for this situation reads

$$\nabla_r^2 u_z = 2\pi s \sum_{\text{creases}} \delta^2(\mathbf{r}-\mathbf{r}_i) - \alpha, \tag{9}$$

where $-\alpha$ is a uniform negative charge density, interpreted as the surface curvature the system would have if the creases were removed (but the compression maintained).

One might ask if this crease-anticrease shape asymmetry could be present even during the KT transition. We suggest the answer is no, because the ghost fiber bound pairs that exist below ϵ_c must have an essentially net zero surface deformation in order to be consistent with the observed "flat" surface. The shape asymmetry is something that arises in connection with the energy penalty for unable-to-self-contact anticreases (but note that other symmetry-breaking mechanisms might also be possible, *e.g.*, coupling to an underlying curvature). One might also ask if there exist conditions in which a system of *anticreases* in a neutralizing *positive* background is realized. Tentative support for this idea comes from recently observed ridges [27], which are somewhat reminiscent of anticreases.

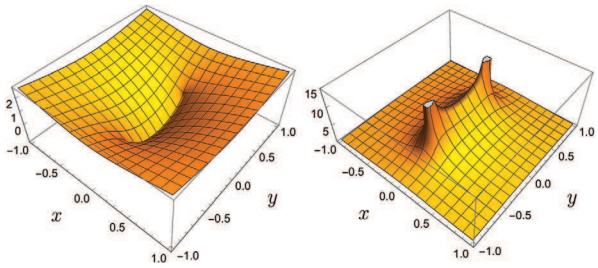

Fig. 2: (Colour online) Deformation field u_z (left panel) and energy density $(\nabla u_z)^2$ (right panel) associated with a finite-length ghost slab, for $\alpha = 0$. Arbitrary units are used for the vertical axes while the horizontal axes are in units of ℓ. The two peaks in the energy density are cut off for visualization purposes, however, they are not singularities.

Ghost slabs. – Having considered ghost fibers, we now consider a thin "ghost slab" of length 2ℓ and height h characterized by charge density $\rho \sim \delta(x)[H(y+\ell) - H(y-\ell)]/R$. (The case $\alpha \neq 0$ will be treated momentarily). A straightforward application of Green's method yields material deformation

$$\begin{aligned} u_z(\mathbf{r}) \sim\ & (y+\ell)\ln\left[(y+\ell)^2+x^2\right] + 2x\tan^{-1}\left(\frac{y+\ell}{x}\right) \\ & - (y-\ell)\ln\left[(y-\ell)^2+x^2\right] - 2x\tan^{-1}\left(\frac{y-\ell}{x}\right), \\ & + \text{constant}, \end{aligned} \tag{10}$$

and strain energy density

$$\begin{aligned} (\nabla u_z)^2 \sim\ & \left[\tan^{-1}\left(\frac{y+\ell}{x}\right) - \tan^{-1}\left(\frac{y-\ell}{x}\right)\right]^2 \\ & + \left[\tanh^{-1}\left(\frac{2\ell y}{r^2+\ell^2}\right)\right]^2. \end{aligned} \tag{11}$$

Equations (10) and (11) are plotted in fig. 2 for $\ell = 1/2$. In the thermodynamic limit, the rotational contribution to the ghost slab entropy is insignificant, and the only important contribution to the elastic energy comes from the monopole term. Similar arguments to those used above lead to a critical strain fluctuation for slabs $\langle\epsilon_d^2\rangle_{c,\text{slab}} \sim (\ell^2/\lambda_d^2)\,\overline{\tan^2\theta}$. This result reveals ghost fibers to be a limiting case of ghost slabs (*i.e.*, as $\ell \to R$).

Experiments and simulations employing uniaxial strain tend to generate straight, parallel creases; when the strain is large, the creases can span the system size, forming a 1d array [7,8,16]. Within our electrostatics framework, for $\alpha \neq 0$, surface profiles of such systems are predicted to have the same form as the electrostatic potential of a 1d Coulomb crystal (a periodic stack of infinite, charged sheets embedded in a charge-neutralizing, uniform background). Figure 3(a) shows a test of this prediction.

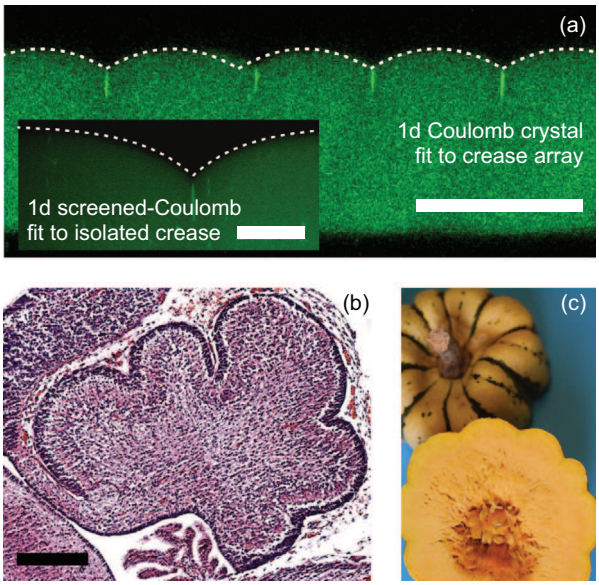

Fig. 3: (Colour online) (a) Confocal microscope image of a 1d crease array in a PDMS elastomer film under 55% uniaxial compression (via attachment to a pre-stretched substrate). Inset: isolated crease in a PDMS film under 46% compression. (Images courtesy of Dayong Chen and Ryan Hayward.) In both images the crease(s) run perpendicular to the plane of the page, the small bright regions are regions of self-contact, and the scale bar indicates 40 microns. The 1d Coulomb crystal fit is of the form $u_z(x_i) \sim x_i - x_i^2/a$, as discussed in the main text, where a is the average crease spacing taken from the experimental image, and x_i is the spatial coordinate within the i-th unit cell. (b) Midline saggital section of a mouse cerebellum at 18.5 embryonic days development, roughly two days after creasing onset (courtesy of Andrew Lawton and Alex Joyner). The scale bar indicates 200 microns. (c) Creasing in a sweet dumpling squash (courtesy of Indian Creek Farm, Ithaca, NY), elsewhere described as wrinkling [41,42].

The possibility of the background being "polarizable" is investigated via the d-dimensional charge screening equation $(\nabla_d^2 - \lambda^{-2})\phi = -4\pi Q\delta^{(d)}$, where Q is the charge and λ is the screening length [43]. The $d = 1$ solution, $\phi(x) \sim e^{-x/\lambda}$, is fit to the profile of an isolated long crease in the inset of fig. 3(a). The qualitative shape of the crease array in fig. 3(a) (parabolic crests between sharp cusps) occurs in other settings such as a mouse cerebellum and a winter squash (fig. 3(b), (c)). Prior work has modeled these as elastic materials [44,45], suggesting the same mechanism may be at play, in spite of the different (curved *vs.* planar) geometry.

Experiments and simulations employing equibiaxial strain tend to generate a square lattice of short, straight creases with each nearest-neighbor pair having relative orientation of 90 degrees; at high strains, a hexagonal lattice of 3-fold symmetric, Y-shaped creases is also seen [16]. (Figure 3(c) in [5] exhibits both motifs.) Within our framework, such patterns again have a natural interpretation as charge-crystallized shear lag quasi-particles. In the limit where the spatial extent of quasi-particles is very small compared with their lattice spacing (*i.e.*, they are ghost fiber-like), the creasing pattern is predicted to be a 2d Coulomb crystal with hexagonal symmetry (*e.g.*, ref. [46]). In fact the hexagonal dimple crystal observed in [28] is suggestive of this, and further, the authors characterize these dimples as being quasi-particles with mutual repulsive interactions. Outside the limit of fiber-like quasi-particles, the ground-state crystal structure is an interesting topic for future work.

Discussion. – Upon building a composite materials-inspired quasi-particle framework, we have found evidence for a micro-creasing scenario that involves at least three distinct regimes. For in-plane compressive strain $\epsilon < \epsilon_c$, the system contains tightly bound pairs of ghost fibers whose deformation fields largely cancel. For $\epsilon_c < \epsilon < \epsilon_{sc}$, the pairs are unbound, giving rise to spatially separated, cusped surface deformations. Also in this regime, zero-length (anti)creases smoothly become finite-length (anti)creases, as ghost fibers smoothly change dimensionality into ghost slabs. For $\epsilon > \epsilon_{sc}$, anticreases smear out into a charge-compensating background, while repulsive interactions between creases causes them to organize into a Coulomb crystal. The KT transition is predicted to occur at a universal critical strain $\epsilon_c \approx 30\%$ (renormalization group analysis) and self-contact is expected to commence at a slightly higher strain ϵ_{sc}. Both transition points should be observable, by virtue of the characteristics of the regimes they delineate (*e.g.*, surface profiles), providing a means for experimental tests of our theory.

Additionally, numerical and experimental work could be undertaken to test our postulate of an effective temperature arising from non-affine fluctuations. While eq. (5) is appealing in that it leads to a critical point independent of shear modulus and system thickness, as well as a reasonably accurate value for the onset strain within the approximation scheme described above, it is possible that the effective temperature has a different form, or that there is no effective temperature. Some starting points would be to investigate the time-dependence of non-affine fluctuations and to look for telltale fluctuation-dissipation violations.

High-resolution imaging will be important for accessing the proposed micro-crease regime, where the characteristic lengthscale is set by non-affine fluctuations of the inherently disordered polymer network. We re-emphasize the presence of this fundamental lengthscale in our theory of micro-creases, which is in contrast to prior work claiming the creasing instability is scale-free [21,22].

Finally, independence of ϵ_c from shear modulus and system thickness suggests that creasing is, in its most general form, an interface phenomenon between dissimilar elastomers or gels, and that creasing of a free surface is merely a special case. The concepts of crease and anticrease naturally generalize to an interface: a crease in material A can equally well be viewed as an anticrease in material B,

and vice versa (see, *e.g.*, ref. [47]). In the electrostatic picture, the essential difference between surface and interfacial creasing is in the behavior of the charge density $2\pi R \tan(\theta(z))$. For surface creasing, $\tan\theta$ is a monotonically increasing (or decreasing) function of z, whereas for interfacial creasing, $\tan\theta$ goes through a maximum (or minimum) at the interface. All the interesting 2d Coulomb gas physics is contained in the z-averaged Poisson equation, however, rendering these details unimportant.

* * *

The authors are grateful to Ryan Hayward, Joseph Paulsen, and Teng Zhang for helpful discussions, and thank several anonymous referees for providing useful comments on the manuscript. TAE and JMS acknowledge financial support from NSF-DMR-CMMT Award No. 1507938.

REFERENCES

[1] Li B., Cao Y.-P., Feng X.-Q. and Gao H., *Soft Matter*, **8** (2012) 5728.
[2] Southern E. and Thomas A. G., *J. Polym. Sci.*, **3** (1965) 641.
[3] Gent A. N. and Cho I. S., *Rubber Chem. Technol.*, **72** (1999) 253.
[4] Tanaka T., Sun S.-T., Hirokawa Y., Katayama S., Kucera J., Hirose Y. and Amiya T., *Nature*, **325** (1987) 796.
[5] Trujillo V., Kim J. and Hayward R. C., *Soft Matter*, **4** (2008) 564.
[6] Yoon J., Kim J. and Hayward R. C., *Soft Matter*, **6** (2010) 5807.
[7] Cai S., Chen D., Suo Z. and Hayward R. C., *Soft Matter*, **8** (2012) 1301.
[8] Chen D., Cai S., Suo Z. and Hayward R. C., *Phys. Rev. Lett.*, **109** (2012) 038001.
[9] Chen D., Jin L., Suo Z. and Hayward R. C., *Mater. Horiz.*, **1** (2014) 207.
[10] Liang X., Tao F. and Cai S., *Soft Matter*, **12** (2016) 7726.
[11] Tallinen T., Chung J. Y., Biggins J. S. and Mahadevan L., *Proc. Natl. Acad. Sci. U.S.A.*, **111** (2014) 12667.
[12] Tallinen T., Chung J. Y., Rousseau F., Girard N., Lefèvre J. and Mahadevan L., *Nat. Phys.*, **12** (2016) 588.
[13] Tang S., Gao B., Zhou Z., Gu Q. and Guo T., *Soft Matter*, **13** (2017) 619.
[14] Hong W., Zhao X. and Suo Z., *Appl. Phys. Lett.*, **95** (2009) 111901.
[15] Cai S., Bertoldi K., Wang H. and Suo Z., *Soft Matter*, **6** (2010) 5770.
[16] Tallinen T., Biggins J. S. and Mahadevan L., *Phys. Rev. Lett.*, **110** (2013) 024302.
[17] Fernández V., Llinares-Benadero C. and Borrell V., *EMBO J.*, **35** (2016) 1021.
[18] Cerda E. and Mahadevan L., *Phys. Rev. Lett.*, **90** (2003) 074302.
[19] Huang J., Juszkiewicz M., de Jeu W. H., Cerda E., Emrick T., Menon N. and Russell T. P., *Science*, **317** (2007) 650.
[20] Paulsen J. D., Hohlfeld E., King H., Huang J., Qiu Z., Russell T. P., Menon N., Vella D. and Davidovitch B., *Proc. Natl. Acad. Sci. U.S.A.*, **113** (2016) 1144.
[21] Hohlfeld E. and Mahadevan L., *Phys. Rev. Lett.*, **106** (2011) 105702.
[22] Hohlfeld E. and Mahadevan L., *Phys. Rev. Lett.*, **109** (2012) 025701.
[23] Ben Amar M. and Ciarletta P., *J. Mech. Phys. Solids*, **58** (2010) 935.
[24] DiDonna B. A. and Lubensky T. C., *Phys. Rev. E*, **72** (2005) 066619.
[25] Wen Q., Basu A., Janmey P. A. and Yodh A. G., *Soft Matter*, **8** (2012) 8039.
[26] Kosterlitz J. M. and Thouless D. J., *J. Phys. C: Solid State Phys.*, **6** (1973) 1181.
[27] Takei A., Jin L., Hutchinson J. W. and Fujita H., *Adv. Mater.*, **26** (2014) 4061.
[28] Brojan M., Terwagne D., Lagrange R. and Reis P. M., *Proc. Natl. Acad. Sci. U.S.A.*, **112** (2015) 14.
[29] López Jiménez F., Stoop N., Lagrange R., Dunkel J. and Reis P. M., *Phys. Rev. Lett.*, **116** (2016) 104301.
[30] Cox H. L., *Brit. J. Appl. Phys.*, **3** (1952) 72.
[31] Hull D. and Clyne T. W., *An Introduction to Composite Materials*, 2nd edition (Cambridge University Press) 1996.
[32] Kardar M., *Statistical Physics of Fields* (Cambridge University Press) 2007.
[33] Bi D., Henkes S., Daniels K. E. and Chakraborty B., *Annu. Rev. Condens. Matter Phys.*, **6** (2015) 63.
[34] Cugliandolo L. F., *J. Phys. A: Math. Theor.*, **44** (2011) 483001.
[35] Casas-Vázquez J. and Jou D., *Rep. Prog. Phys.*, **66** (2003) 1937.
[36] Nisoli C., Li J., Ke X., Garand D., Schiffer P. and Crespi V. H., *Phys. Rev. Lett.*, **105** (2010) 047205.
[37] Kolton A. B., Exartier R., Cugliandolo L. F., Domínguez D. and Grønbech-Jensen N., *Phys. Rev. Lett.*, **89** (2002) 227001.
[38] Lindemann F. A., *Z. Phys.*, **11** (1910) 609.
[39] Shimizu I., Abe T., Nosho T. and Wakayama M., *Met. Mater.*, **4** (1998) 939.
[40] Minnhagen P., *Rev. Mod. Phys.*, **59** (1987) 1001.
[41] Yin J., Cao Z., Li C., Sheinman I. and Chen X., *Proc. Natl. Acad. Sci. U.S.A.*, **105** (2008) 19132.
[42] Wang Q. and Zhao X., *Sci. Rep.*, **5** (2015) 8887.
[43] Johnson-McDaniel N. K. and Owen B. J., *Phys. Rev. D*, **86** (2012) 063006.
[44] Lejeune E., Javili A., Weickenmeier J., Kuhl E. and Linder C., *Soft Matter*, **12** (2016) 5613.
[45] Hu D. L., Richards P. and Alexeev A., *Int. J. Nonlinear Mech.*, **46** (2011) 637.
[46] Bonitz M., Ludwig P., Baumgartner H., Henning C., Filinov A., Block D., Arp O., Piel A., Käding S., Ivanov Y., Melzer A., Fehske H. and Filinov V., *Phys. Plasmas*, **15** (2008) 055704.
[47] Jin L., Chen D., Hayward R. C. and Suo Z., *Soft Matter*, **10** (2014) 303.